



1 Generation of autogenic knickpoints in laboratory landscape
2 experiments evolving under constant forcing.

3

4 **Léopold de Lavaissière¹, Stéphane Bonnet¹, Anne Guyez¹, and Philippe Davy²**

5 ¹ GET, Université de Toulouse, CNRS, IRD, UPS(Toulouse), France,

6 ² Univ Rennes, CNRS, Géosciences Rennes - UMR 6118, 35000 Rennes, France,

7 Correspondance to Léopold de Lavaissière (leopold.delavaissiere@gmail.com)

8

9 **ABSTRACT**

10 **The upward propagation of knickpoints in the long profiles of rivers is commonly related to**
11 **discrete changes in tectonics, climate or base-level. However, the recognition that some**
12 **knickpoints may form autogenically, independently of any external perturbation, may challenge**
13 **these interpretations. We investigate here the genesis and dynamics of such autogenic knickpoints**
14 **in laboratory experiments at the drainage basin scale, where landscape evolved in response to**
15 **constant rates of base-level fall and precipitation. Despite these constant forcing, we observe that**
16 **knickpoints regularly initiate in rivers at the catchments' outlets throughout experiments**
17 **duration. Their propagation rate does not decrease monotonically in relationship with the**
18 **decrease in drainage area as predicted by stream-power based models, but first increases with a**
19 **peak retreat rate in the mid-part of catchments. Their initiation coincides with rivers narrowing**
20 **and increasing their shear stress. Then, rivers widening leads to a decrease in shear stress and**
21 **incision rate below the base-level fall rate once knickpoints have propagated upward, creating an**
22 **unstable situation that ends up with the formation of a new knickpoint. We propose a new model**
23 **of cyclic generation of autogenic knickpoints controlled by river width dynamics. It illustrates the**
24 **need to consider autogenic processes in the generation of knickpoints and for deciphering**
25 **variation of tectonic and climatic processes from landscape records.**



26 **1 Introduction**

27 Knickpoints in rivers are discrete zones of steepened bed gradient that are commonly observed in their
28 long profiles. Although they occasionally occur due to changes in bedrock properties (e.g. Duvall et al.,
29 2004), in many cases they are dynamical features that propagate upstream along the drainage network
30 of landscapes (Whipple and Tucker, 1999; Kirby and Whipple, 2012; Whittaker and Boulton, 2012;
31 Yanites et al., 2013). In this last case, they are commonly considered as formed in response to variations
32 in external forcing such as uplift rate, sea-level or climate. According to a stream-power based celerity
33 model (SPCM), their upstream propagation rate is predicted to depend non-linearly on drainage area (a
34 proxy for discharge; Crosby and Whipple 2006; Berlin and Anderson, 2007), implying a monotonous
35 decrease of retreat rate as they propagate upstream. This property can be used for example to invert their
36 present location for dating the external perturbation responsible for their formation (Crosby and Whipple
37 2006; Berlin and Anderson, 2007). A recent experimental study however pointed out a potential
38 inadequacy of this model when the upstream decrease in discharge is counterbalanced by the adjustment
39 of the river width, resulting in a constant knickpoint retreat rate (Baynes et al., 2018). Some other studies
40 also pointed out some limitation of SPCM to predict the actual propagation of knickpoints when the role
41 of sediment supply is not considered (Cook et al., 2013).

42 Unlike the commonly accepted idea that knickpoints are symptomatic of changing external forcing (e.g.
43 Crosby and Whipple 2006; Berlin and Anderson, 2007; Kirby and Whipple, 2012; Whittaker and
44 Boulton, 2012; Mitchell and Yanites, 2019), several studies pointed out that they could also be
45 autogenic, that is to say internally-generated without any variation in boundary condition (e.g.
46 Hasbargen and Paola, 2000, 2003; Finnegan and Dietrich, 2011). Their consideration should then be
47 crucial for retrieving changes in external forcing from analysis of knickpoints observed in landscapes.
48 Autogenic knickpoints has been observed for example in experimental drainage basins forced by
49 constant rate of base-level (BL) fall by Hasbargen and Paola (2000). In their experiments, successive
50 knickpoints initiated despite constant forcing, even when landscapes were at steady-state. Internal
51 processes may also complexify the propagation of knickpoints as shown in flume experiments by
52 Cantelli and Muto (2014) and Grimaud et al. (2016) who observed that a single discrete event of BL



53 drop may result in the propagation of multiple knickpoints. Other flume experiments show that some
54 knickpoints may generate autogenically along a river profile from the amplification of local instabilities
55 (Scheingross et al., 2019).

56 We consider here the generation and dynamics of autogenic knickpoints in laboratory-scale drainage
57 basins experiments forced by constant rate of BL fall and steady precipitation. We observe that
58 successive knickpoints initiate near the outlet and propagate within drainage basins and propose a new
59 model of autogenic knickpoint initiation and propagation driven by downstream river width dynamics.

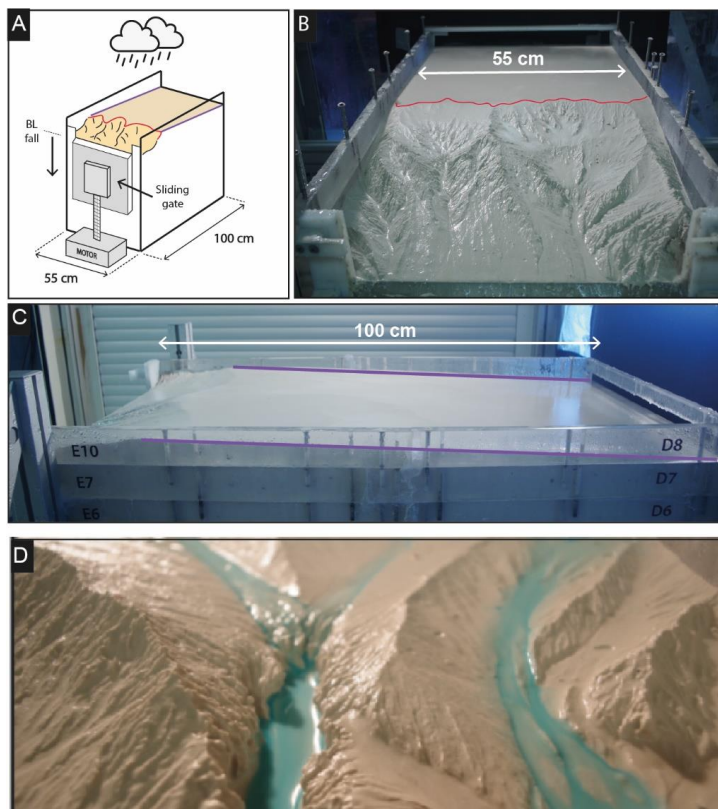
60

61 **2 Methods**

62 Landscape experiments have been used successfully to explore how tectonics and climate impact erosion
63 processes and the evolution of topography under controlled conditions (e.g. Hasbargen and Paola, 2000;
64 Bonnet and Crave, 2003; Lague et al., 2003; Turowski et al., 2006; Bonnet, 2009; Singh et al., 2015;
65 Sweeney et al., 2015; Moussirou and Bonnet, 2018). This approach allows the observation of complex
66 dynamics that are difficult to simulate numerically and sheds new light on the way natural landforms
67 may evolve. The experiments presented here have been performed using a new setup specifically
68 designed to investigate landscape evolution under controlled BL fall (Fig. 1; see also Fig. S1 in the
69 Supplemental Material). The facility is a box with dimensions 100 x 55 cm filled with silica paste. At
70 its front side, a sliding gate, 41 cm-wide, drops down at constant rate, acting as the BL. During a run,
71 runoff-induced erosion occurs in response to steady artificial rainfall (95 mm.h^{-1}) and BL fall. Then,
72 some incisions initiate along the BL and propagate up to a complete dissection of the initial surface,
73 which consists on a plane with a counterslope of $\sim 3^\circ$, opposite to the BL-side. This allows to create a
74 water divide between incisions that develop along the BL-side and the initial surface. The use here of a
75 large gate on the BL-side of the setup constitutes a major difference compared to previous similar
76 catchment-scale experiments of Hasbargen and Paola (2000, 2003), Bigi et al. (2006) and Rohais et al.
77 (2012). In these experiments, a single outlet location was actually pinned due a narrow gate, which also



78 set the river width at the outlet. Unlike these experiments, the setup use here allows experimental rivers
79 to freely evolved, with their width not being constrained by such a narrow gate.



80

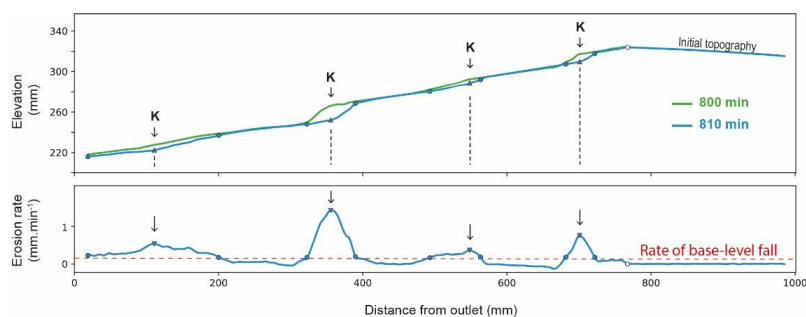
81 **Figure 1.** *Experimental setup. Purple and red lines show respectively the counter-slope of the initial*
82 *topography and the main water divide. (A) Sketch of the erosion box with the sliding gate, 41 cm wide,*
83 *used to drop down base level (BL). (B), (C) Front and side photographs (experiments MBV07 at 525'*
84 *and MBV06 at 185'). (D) Photograph of a typical knickpoint studied here.*

85

86 Experiments were stopped every 5 min to digitize the topography using a laser sheet and to construct
87 DEMs with a pixel size of 1 mm. Due to the large number of DEMs per experiment, about 200, river
88 long profiles and knickpoints were extracted based on a semi-automatic procedure. For this purpose, we
89 first extracted long profiles by considering the lowest elevation on the successive rows of each DEM



90 within a 20 cm-wide swath that included the main river and then by plotting it against distance down
91 the long axis of the box. This procedure has already been applied in analysis of experiments by Baynes
92 et al. (2018) and Tofelde et al. (2019). It may result in a slight overestimation in channel slope because
93 it does not consider the obliquity of channels within the box in the distance calculation nor their
94 sinuosity, however these effects are of minor influence here, most of channels being straight and roughly
95 parallel to the long side of the box. In a second step, we computed the elevation difference between
96 each successive pairs of longitudinal profiles and we identified knickpoints by considering peaks in
97 erosion with values above the steady erosion amount defined by the rate of base-level fall (Fig. 2). We
98 carefully verified manually that this procedure allows to define knickpoints correctly and we
99 investigated in particular how the procedure performed according the time interval chosen between
100 successive profiles. We found that knickpoint retreats were generally too small to produce well-defined
101 erosional peaks when we considered the highest time-resolution of 5 minutes, which lead us to track
102 knickpoint positions at a time-interval of 10 minutes. Thanks to this approach, we built a first rough
103 catalogue of knickpoints positions over time that we subsequently rearranged manually by gathering
104 together the successive positions of each individual knickpoint. We then complemented the database by
105 computing incremental retreat rate of knickpoints from their successive positions.



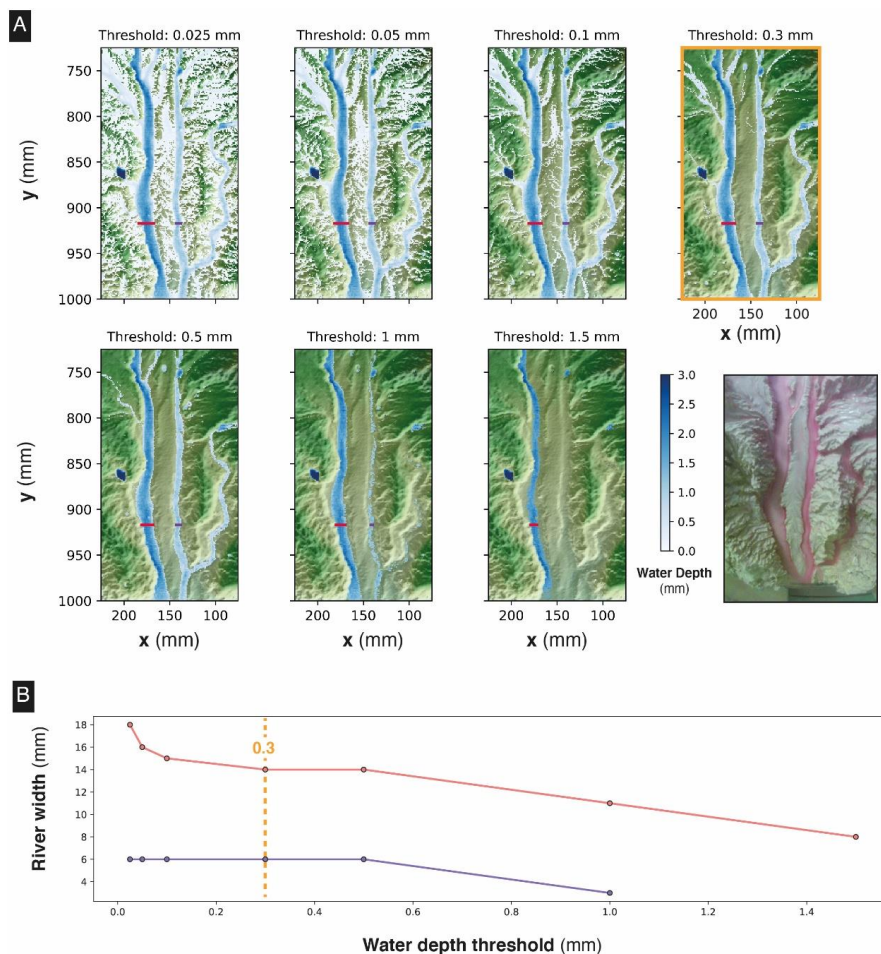
106

107 **Figure 2.** Graph showing two successive long profiles of experiment MBV07 taken at 10 min interval
108 (top) and corresponding erosion rate profile (bottom). Triangles illustrate the position of erosional
109 peaks taken as knickpoint position (black arrows). Red dashed line shows the rate of base-level fall.

110



111 DEMs were also used to compute hydraulic information (water depth, river width, discharge and shear
112 stress; see Supplemental Material) using the Floodos hydrodynamic model of Davy et al. (2017; see
113 also Baynes et al. (2018, 2020) for previous use of Floodos for analyzing laboratory experiments).
114 Floodos is a precipitation-based model that calculates the 2D shallow water equations (SWE) without
115 inertia terms, from the routing of elementary water volumes on top of topography. The output of
116 floodos are maps of water depth, velocity and shear stresses. We ran Floodos on successive DEMs of
117 experiments by considering spatial distribution of precipitation, then generating several output raster
118 products at the pixel size, including water depth, unit discharge and bed shear stress that were then
119 used for computation of hydrologic parameters (river width, specific discharge and shear stress). The
120 solution of the SWE depends on the friction coefficient (C) that depends on water viscosity only for
121 laminar flow; its theoretical value is $\sim 2.5 \times 10^6 \text{ m}^{-1} \cdot \text{s}^{-1}$ at 10°C (Baynes et al., 2018). To ensure that
122 Floodos outputs (e.g. water depth raster maps) calculated using this value are consistent with actual
123 experiment hydraulic conditions, we injected dye in the rainfall water during a run to catch the actual
124 extent of water flow and make rivers visible (see Fig. 2 and Fig. S2). A visual comparison with
125 Floodos results shows a good match between model outputs and experimental results, which validates
126 the numerical method and the expected theoretical friction coefficient C (Baynes et al., 2018). River
127 widths were extracted from DEMs by considering water depth maps and a threshold depth between
128 channels and hillslopes. Floodos routing procedure calculates water depth from precipitation over the
129 totality of the topography, on hillslopes as well as in channels, river banks corresponding to sharp
130 variations in water depth. During runs, the actual water depth in rivers is very low, of mm-scale, and
131 very difficult to measure without introducing any perturbation in the flow. Thus, the water depth
132 threshold was estimated by varying this threshold over a DEM and by comparing the corresponding
133 extent of rivers with actual extent of water flow as viewed by injecting red dye in the water used to
134 produce the artificial rainfall (Fig. 3). A good visual agreement was obtained for a threshold value
135 between 0.1 and 0.5 mm, and a mid-value of 0.3 mm was consecutively used for determining river
136 widths.
137



138

139 **Figure 3.** Impact of water depth threshold used to delineate river boundaries on estimated river widths,
 140 considering a friction coefficient C of $2.5 \times 10^6 \text{ m}^{-1} \text{ s}^{-1}$. A. Map views of water depths (blue colors)
 141 superimposed to DEM, for water depths threshold values between 0.025 and 1.5 mm. Red and purple
 142 lines show corresponding river widths for two rivers. Photo on the bottom right shows the active river
 143 width during the corresponding experimental run (pink colors; “control run”), viewed by injecting red
 144 dye in the water used to generate the artificial rainfall. B. Corresponding local river widths for the two
 145 sections shown by red and purple lines. The use of a low water depth threshold value (e.g. 0.025 mm;
 146 top left) leads to the inclusion of large areas of thin water depth in the “wetted area” considered as
 147 rivers and then to unrealistic large rivers in comparison with actual rivers observed in the control run.



148 *On the opposite, considering large threshold value (e.g. 1.5 mm) results in narrow rivers, or even in the*
149 *absence of rivers when maximum computed water depth is lower than the threshold used. A threshold*
150 *value of between 0.1 and 0.5 mm shows a good similarity between rivers on water depth map and the*
151 *control run. Here, a mid-value of 0.3 mm has been chosen for computing river widths.*

152

153 **3 Results**

154 **3.1 Dynamics of knickpoints retreat**

155 We present here results from 3 experiments, MBV09, MBV07 and MBV06, performed with different
156 rates of BL fall, of respectively 5, 10 and 15 mm.h⁻¹ (Table 1). In each experiment, BL fall induces the
157 growth of drainage networks by headward erosion and the progressive migration of a main water divide
158 (Fig. 4). The migration rate of the divide is constant in each experiment (Fig. 5 and Table 1), but
159 increases from 25 to 66 mm.h⁻¹ for increasing rate of BL fall. Figure 6 shows the evolution of the
160 longitudinal profile of the main river investigated in each experiment, as well as topography of the initial
161 surface, the profiles being colored according to the experimental runtime. These stacks illustrate the
162 growth of rivers as they propagate within the box. Longitudinal profiles show alternations of segments
163 with low and higher slopes, the later defining knickpoints that propagate upward, some profiles showing
164 even several knickpoints that retreat simultaneously. Knickpoints regularly initiate at the outlet
165 throughout the duration of the runs in all experiments, and propagate upward until they reach and merge
166 with the divide. The mean retreat velocity of knickpoints varies between experiments from 73 ± 50 to
167 183 ± 94 mm.h⁻¹ (Table 1) and increases in average as a function of the rate of BL fall. Data suggest a
168 non-linear relationship however complementary experiments would be necessary to constraint this
169 dependency. To investigate the propagation of the knickpoints, we show in Figure 7 the successive
170 alongstream position of each knickpoint over experimental runtime, as well as the position of the water
171 divide in the box as already reported in Figure 5. In order to be able to compare the dynamics of
172 knickpoints within an experiment regardless of the stage of water divide retreat into the box, the position
173 of knickpoints (distance to outlet, D) has been normalized to the position of the divide, hereafter referred



174 to as normalized distance to divide (nDD; nDD=0 at outlet and nDD=1 at the divide; Figure 2). Lines
175 of isovalue of nDD considering an increment of 0.1 are also shown in the space-time diagrams in Figure
176 7. To a first order, the trajectories of each knickpoint are very comparable within an experiment whatever
177 regardless the stage of retreat of the water divide and the size of the catchment. Visually for example,
178 in the space-time diagrams there is no systematic variation in the general slope of the successive
179 knickpoint trajectories over time, as the rivers expand, that would indicate a change in mean knickpoint
180 velocity in relation to the change in the river length and catchment size. An inflection of trajectories is
181 visible for many knickpoints when they are close to the divide, for $nDD > \sim 0.8$ (Figure 7), which
182 indicates that they slow down as they approach the divide. The opposite is observed for some
183 knickpoints when they are close to the outlet, for $nDD < \sim 0.2 / 0.3$, with some trajectories suggesting,
184 on the contrary, an acceleration (Figure 7). These suppositions are supported by the detail analysis of
185 retreat velocity data shown in Figure 8. For each experiment, we show in Figure 8A the stack of
186 successive retreat velocities of each individual knickpoint according to nDD, *i.e.* according to their
187 propagation between the outlet and the divide. The envelopes draw a bell-shaped distribution for each
188 experiment, which indicates that retreat velocities are maximum when knickpoints are located at a mid-
189 distance between the outlet and the divide, for central values of nDD, between 0.4 and 0.6. Figure 8b
190 provides summary statistics of retreat velocities at 0.1 intervals of nDD considering all knickpoints in
191 each experiment. Both the mean and median values show higher rates of retreat when knickpoints are
192 in the central section of rivers, and conversely lower rates near the outlet ($nDD < 0.2 / 0.3$) when they
193 initiate and start to propagate and when they approach the divide ($nDD > 0.8$), as suggested by
194 trajectories shown in Figure 7. Then, these data indicate that after their initiation near the outlet,
195 knickpoints first accelerate up and reach their maximum retreat rate in the central part of the catchments
196 before to decelerate as they approach the divide. It is worth noting that this specific distribution of
197 knickpoint retreat rates is observed regardless of the progress of the experiments and the advancement
198 stage of incision and divide retreat into the box. This applies both to rivers in the early stages of evolution
199 of experiments, when they are short, and to very large rivers at the end of evolution of the experiments.

200



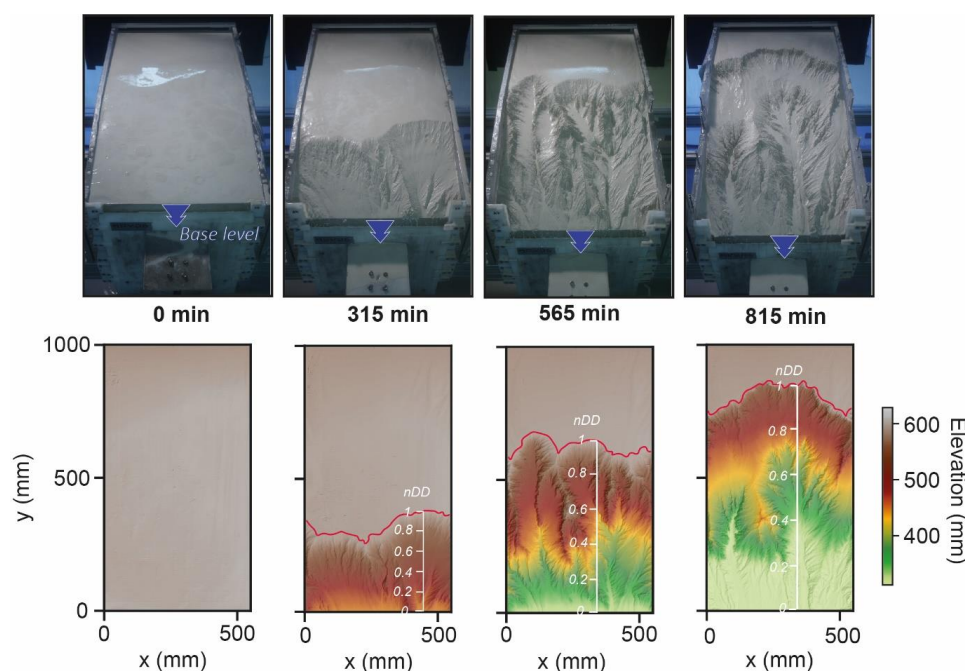
201 **Table 1. Parameters of experiments**

Experiments	Base Level Fall (mm/h)	Precipitation rates (mm/h)	Duration Time (min)	nDDvmax	Mean Knickpoints retreat rates (mm/h)
MBV06	15	95	1065	0.52	183.571 ± 93.784
MBV07	10	95	1200	0.57	164.789 ± 74.8374
MBV09	5	95	1455	0.54	73.127 ± 50.0142

202

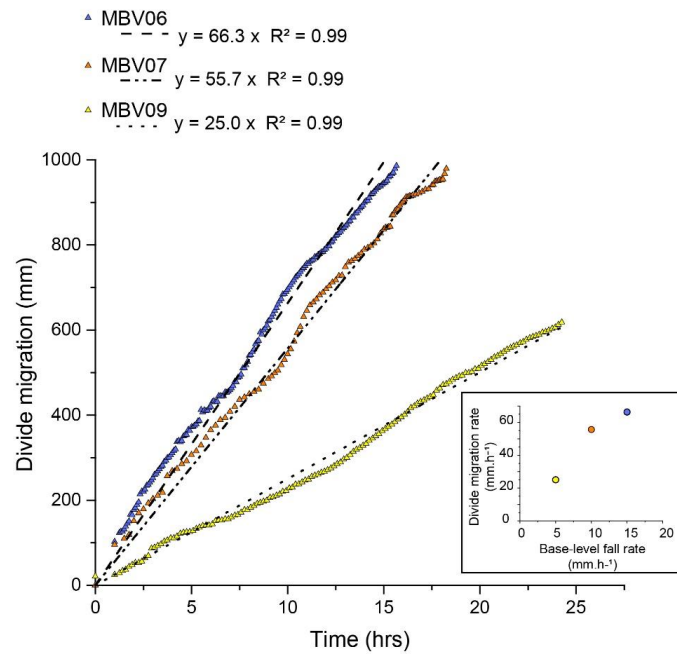
203

204



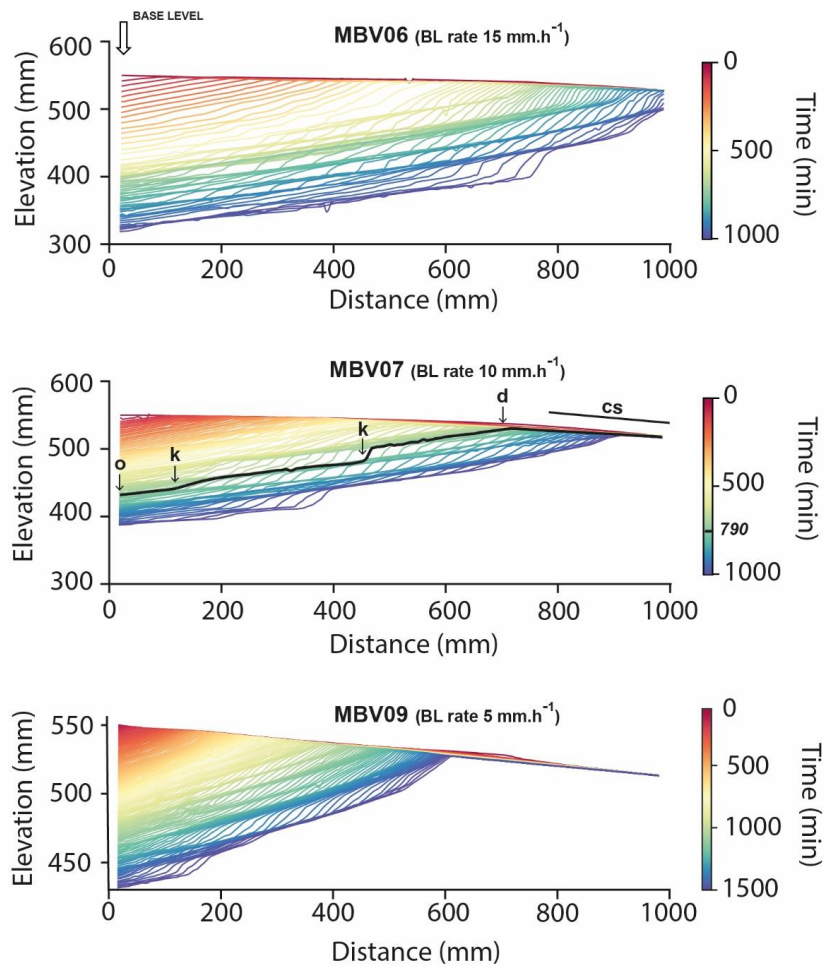
205

206 **Figure 4.** Photos and corresponding DEMs of experiment MBV06 at four runtimes. Note the
 207 propagation of the divide through the erosion box (red line) and the drop of the sliding gate used for
 208 falling base-level. The normalized distance to divide (nDD, see text) used to follow the position of
 209 knickpoints during runs is shown superimposed to DEMs.



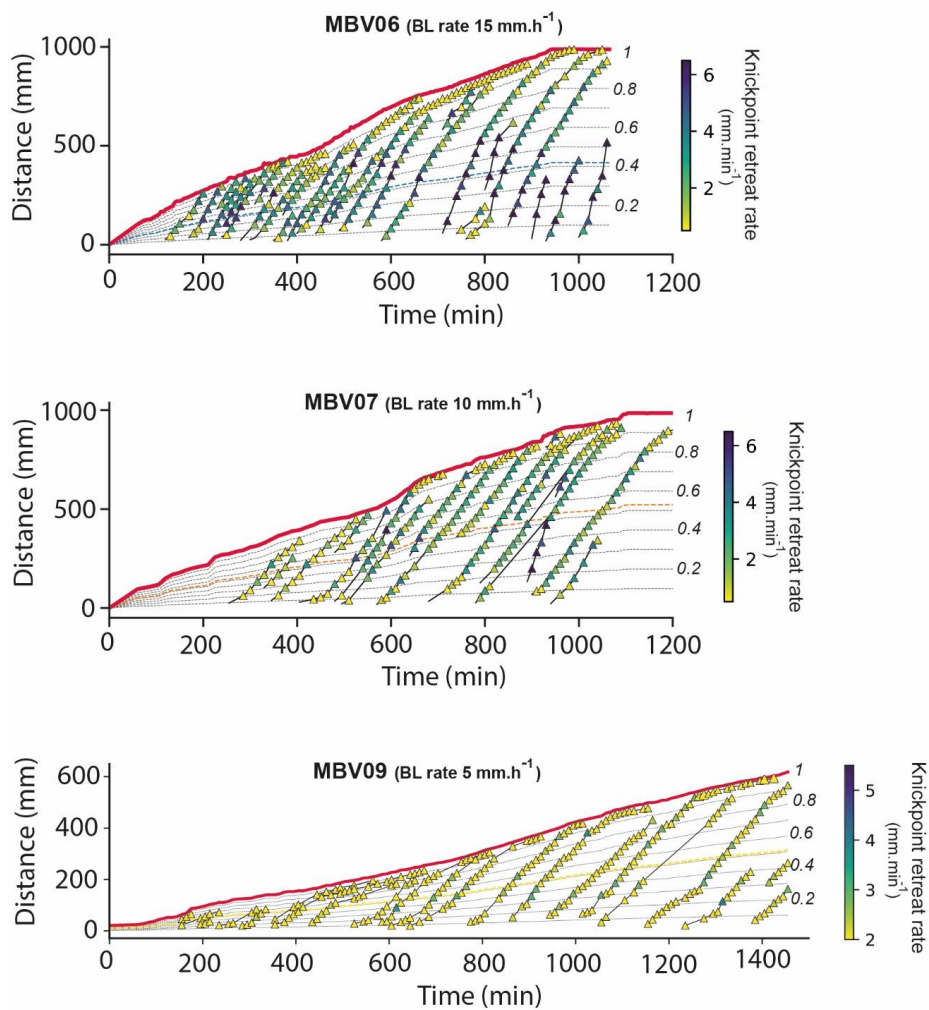
210

211 **Figure 5.** Evolution of the water divide position within the erosion box for the three experiments.



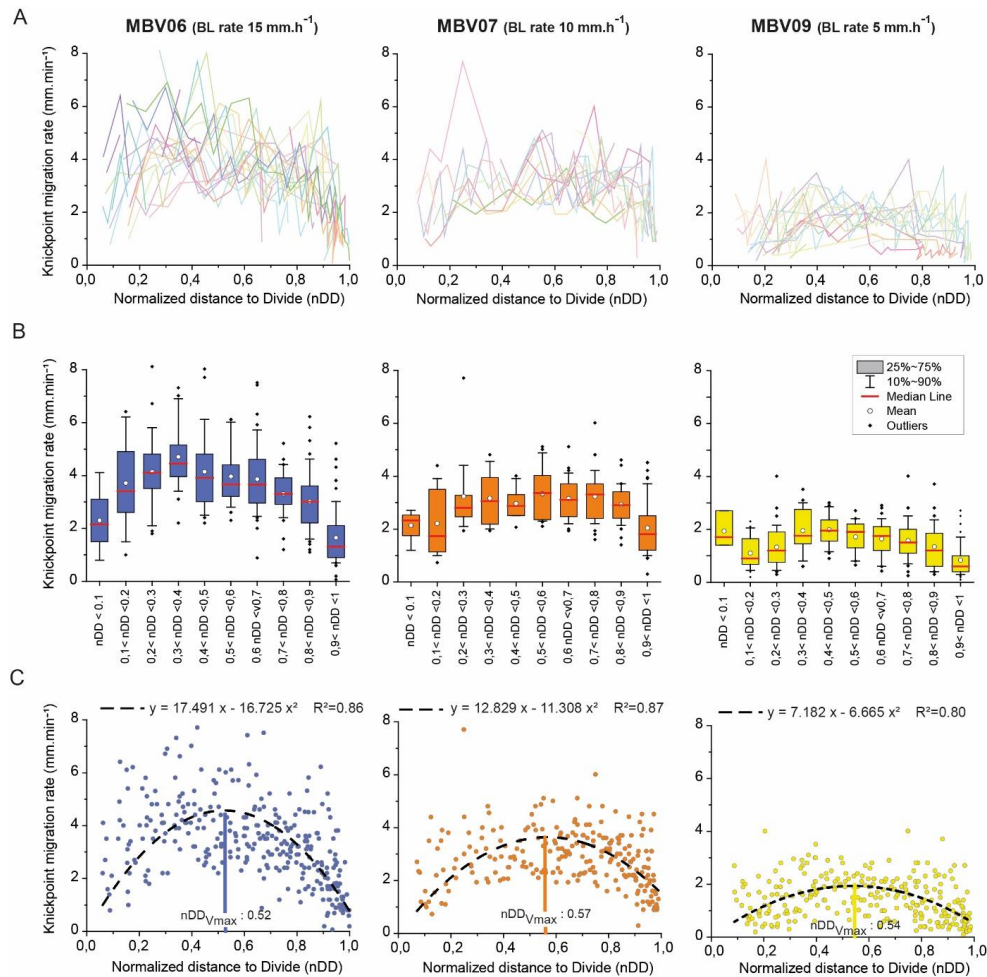
212

213 **Figure 6.** Successive river long profiles of experiments, shown here every 10 min. Each long profile is
214 colored according to experimental runtime. The sliding gate (BL) is to the left. Note the initial
215 counterslope (cs). Black thick line on MBV07 is the long profile at $t=790'$, illustrating the outlet (o),
216 knickpoints (k), and water divide (d).



217

218 **Figure 7.** Space-time diagrams showing the propagation of the water divide (red line) and successive
219 trajectories of knickpoints (triangles). Symbols color shows instant (10 min) knickpoints retreat rate.
220 Thin dashed lines show the normalized distances to divide (nDD).



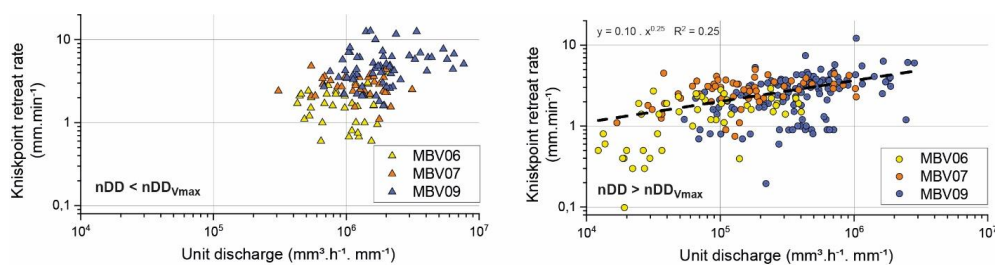
221

222 **Figure 8.** (A) Knickpoint retreat rates according to the normalized distances to divide (nDD) for each
 223 knickpoint of experiments. Each color line corresponds to an individual knickpoint of the space-time
 224 diagram in Fig. 7. (B) Summary statistics of retreat rates for nDD intervals of 0.1. (C) Plot of all
 225 knickpoints retreat rates for each experiment. Black dashed line shows the second order polynomial fit
 226 to the data used to define the normalized longitudinal distance of maximum velocity of knickpoints
 227 (nDD_{Vmax}).

228



229 Studies that investigated knickpoints retreat at catchment-scale demonstrated that their velocity
230 decreases as they propagate upstream due to the progressive reduction of the upstream drainage area
231 and water discharge (e.g. Crosby and Whipple, 2006. Berlin and Anderson, 2007). The pattern of
232 velocity distribution that we document here is not consistent with this finding because we observe here
233 an increase in knickpoints velocity in the early stage of their propagation. To evaluate this effect in our
234 experiments, we investigated the dependency between retreat velocities and discharge by cutting the
235 dataset into two parts corresponding to the different regimes identified above. For this purpose, we
236 considered a second order polynomial fit to the data shown in Figure 8 and used the inflexion to define
237 a normalized longitudinal distance of maximum velocity of knickpoints (Fig. 8C) referred to as $nDD_{V_{max}}$
238 in the following. This value is very similar between experiments, of 0.52 to 0.57 (Table 1). Data above
239 $nDD_{V_{max}}$ (Figure 9) allows to consider retreat rates against more two orders of magnitude of unit
240 discharge (total discharge normalized to river width). They do not show a clear tendency of increasing
241 rate with discharge as expected, although a rough positive correlation could be defined, following a
242 power law with an exponent of 0.25. Data below $nDD_{V_{max}}$ show 3 distinct fields without any clear trend
243 with discharge. The restricted range of discharge data however limits the analysis.



244

245 **Figure 9.** Relationship between knickpoints retreat rates and unit discharge (discharge/width) for nDD
246 $< nDD_{V_{max}}$ (left) and $nDD > nDD_{V_{max}}$ (right).

247

248 3.2 Knickpoints initiation

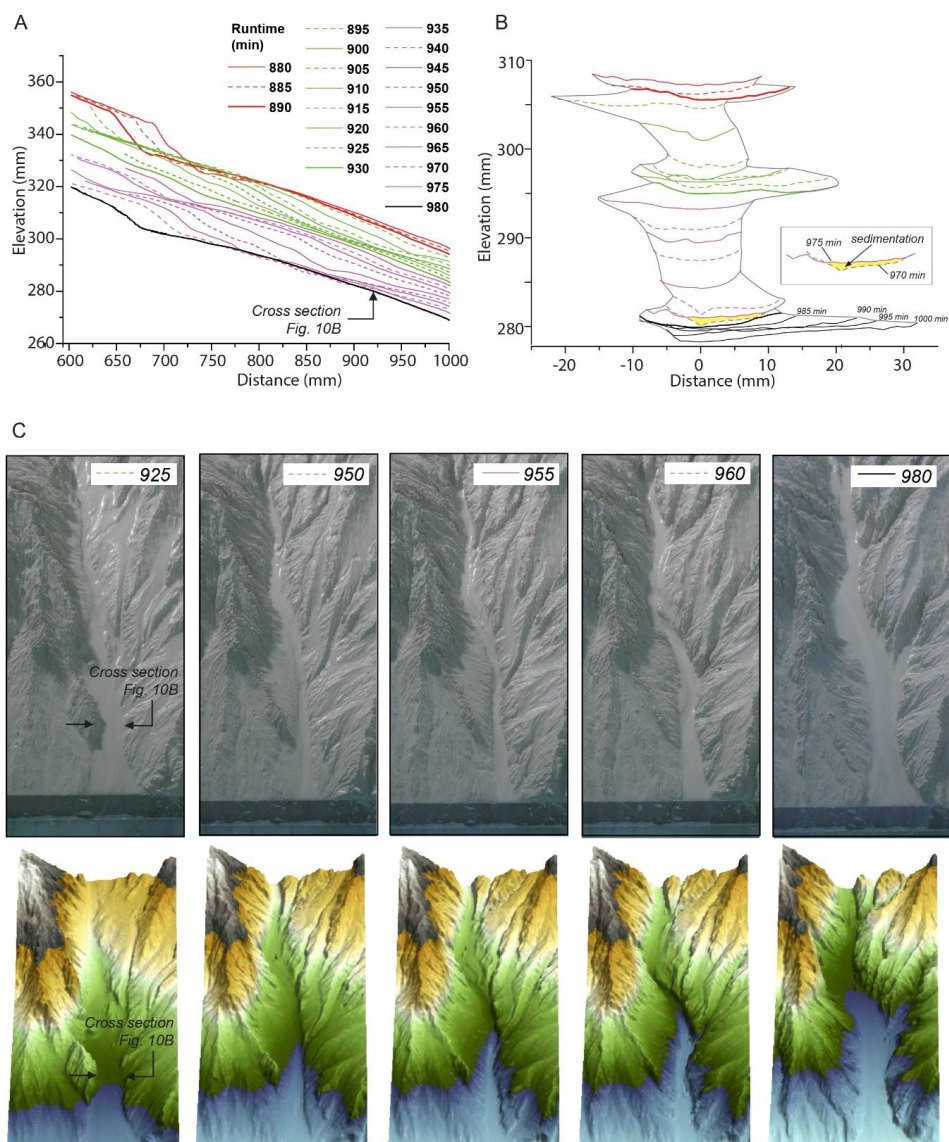
249 To illustrate how knickpoints initiated near the outlet, we consider here a 120 minutes-long sequence of
250 channel evolution in experiment MBV06 from experimental runtime 880 to 1000 minutes, during which



251 two knickpoints successively initiate and propagate upward. Figure 10 shows 5 min intervals sequence
252 of downstream longitudinal profiles, 40 cm-long, showing their initiation and propagation as well as the
253 evolution of a channel cross-section located at 8 cm from the box boundary. Some photos and
254 perspective views of the corresponding DEMs also illustrate the evolution of the channel.
255 Complementary data are shown in Figure 11: variations over time of channel width (Fig. 11A) and unit
256 water discharge (Fig. 11B) at the cross-section location as well as summary statistics of normalized
257 elevation changes (Fig. 11C) and shear stress (Fig. 11D) for all pixels across the section. On the graph
258 shown in Figure 11C, normalized values of 1 indicate erosion at the same rate than base-level fall and
259 then steady-state conditions. Values > 1 or < 1 indicate respectively higher and lower erosion rate than
260 BL fall rate. Negative values indicate sedimentation. The sequence starts with a regular profile at
261 runtimes 880 and 890 min once a knickpoint has already retreated, still visible upstream (Figure 10A).
262 The channel is 23 to 25 mm wide (Fig. 10B and 11A) and unit discharge is about $1.5 \cdot 10^6 \text{ mm}^3 \cdot \text{h}^{-1} \cdot \text{mm}^{-1}$.
263 Erosion in the channel is in average lower than BL fall as normalized erosion is < 1 for most pixels
264 along the section (Fig. 11B). Then, the first knickpoint initiates and starts to retreat. The channel
265 narrows, being ~15 mm wide at 905 min (~60 % decrease), before to subsequently widens once the
266 knickpoint has retreated, at 910 min at the location of the section surveyed (Fig. 10B). The narrowing
267 phase goes with an increase in unit discharge (Fig. 11B) and with an enhanced erosion well above the
268 BL fall rate, up to 4 times this rate in average at 900 min (Fig. 11 C), with extremes as high as 8 times
269 the BL rate. Once this first knickpoint has retreated, unit discharge decreases as the channel subsequently
270 widens, to reach a width of 25 cm to 28 cm between 925 and 930 min (Fig. 11A) while a new regular
271 profile, i.e. without any slope break, established at 930 min (Fig. 10A). The normalized erosion across
272 the section decreased below the BL value (Fig. 11C), with mean erosion rates value of 0.53, 0.36 and
273 0.76 times below the BL rates between 915 to 925 min. Longitudinally, the profiles stack together
274 downstream the knickpoint following its retreat from 895 to 925 min (Fig. 10A), which also indicates
275 minor vertical erosion here once the knickpoint has retreated despite the ongoing falling base-level. A
276 second knickpoint then initiated at 935 min and propagated upstream in a similar way, until
277 establishment of a new regular profile at 980 min (Fig. 10A). The passage of this second knickpoint also
278 coincides with a narrowing of the channel, being ~15 mm wide on the cross-section shown here (Fig.



279 10B and 11A), a rise in the unit discharge and with an increase of the normalized erosion above the BL
280 rate (Fig. 11C). It is followed again by a phase of widening to reach a width to around 30 / 35 mm once
281 the knickpoint has propagated upstream and by a decreasing erosion below the BL fall rate (Fig. 11C).
282 Note that at 975 min, sedimentation took place on a large part of the surveyed section (mean normalized
283 erosion rate is 0.1 and median is -0.25): Figures 10B and 11C. Again, the longitudinal profiles stack
284 together downstream the knickpoint (Fig. 10A). Figure 11D provides summary statistics of shear stress
285 exerted on the channel bed for all pixels along the channel section. The values of shear stress show a
286 quite large variability at the scale of the cross-section, with the median and maximum values increasing
287 however in phase with the passage of knickpoints. Then once passed, shear stress values decrease as the
288 river widens. This sequence illustrates that the rivers are never in equilibrium at the 5 min time-scale,
289 but continuously oscillate over time between periods of disequilibrium during which erosion in wide
290 channels goes at a slower rate than the BL and periods of knickpoint propagation with enhanced erosion
291 and increased discharge in narrower rivers, erosion being well above the BL rate along the knickpoint
292 segment. These knickpoints then propagate upward up to the divide as discussed previously (Fig. 6).
293 Although erosion appears to be fundamentally punctuated over time, considering all erosion rates data
294 across the investigated cross-section and for the whole sequence shown here gives an average
295 normalized erosion rate closed to unity (0.99) which indicates that these oscillations take place however
296 around an average steady state over the long time-scale (erosion rate equal to BL rate). It indicates that
297 enhanced erosion above the BL value during the retreat of knickpoint compensates the delay in vertical
298 erosion that accumulates between two successive knickpoints, while rivers are defeated in following BL
299 fall.



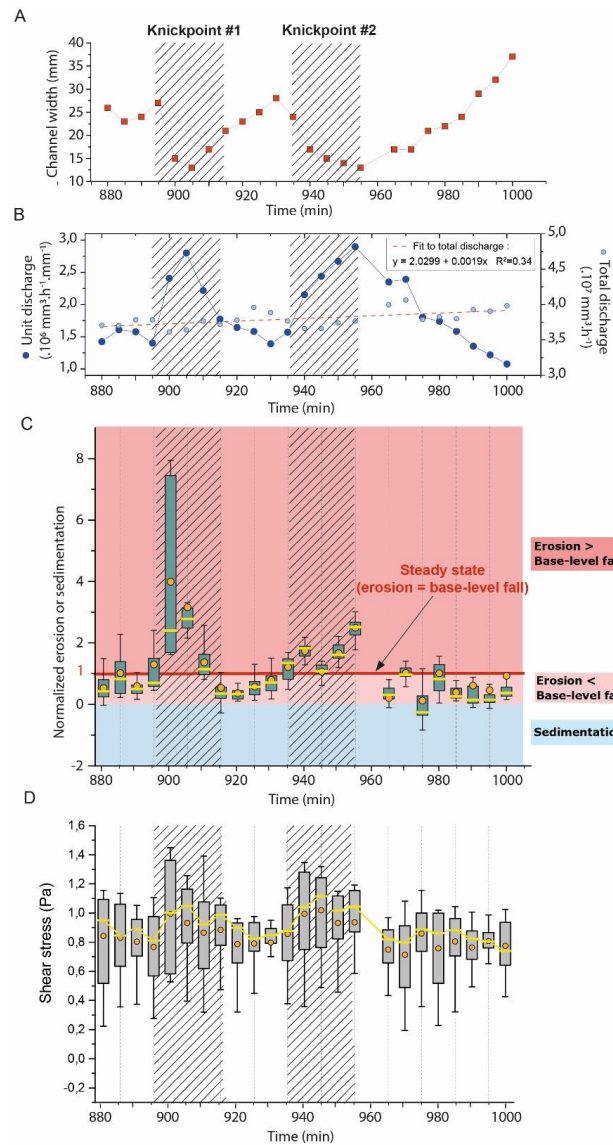
300

301 **Figure 10.** (A) Successive longitudinal profiles (downstream section) of the investigated river in
 302 experiment MBV06, corresponding to the sequence hydro-geomorphic parameters shown in Figures 11
 303 and 12. Propagation of the first (K1) and second (K2) knickpoints is shown in blue and orange colors
 304 respectively (see text). (B) Time evolution of successive cross-sections of the channel at 80 mm from the
 305 outlet. (C) Photos and perspective views of DEM at five time-steps.

306



307

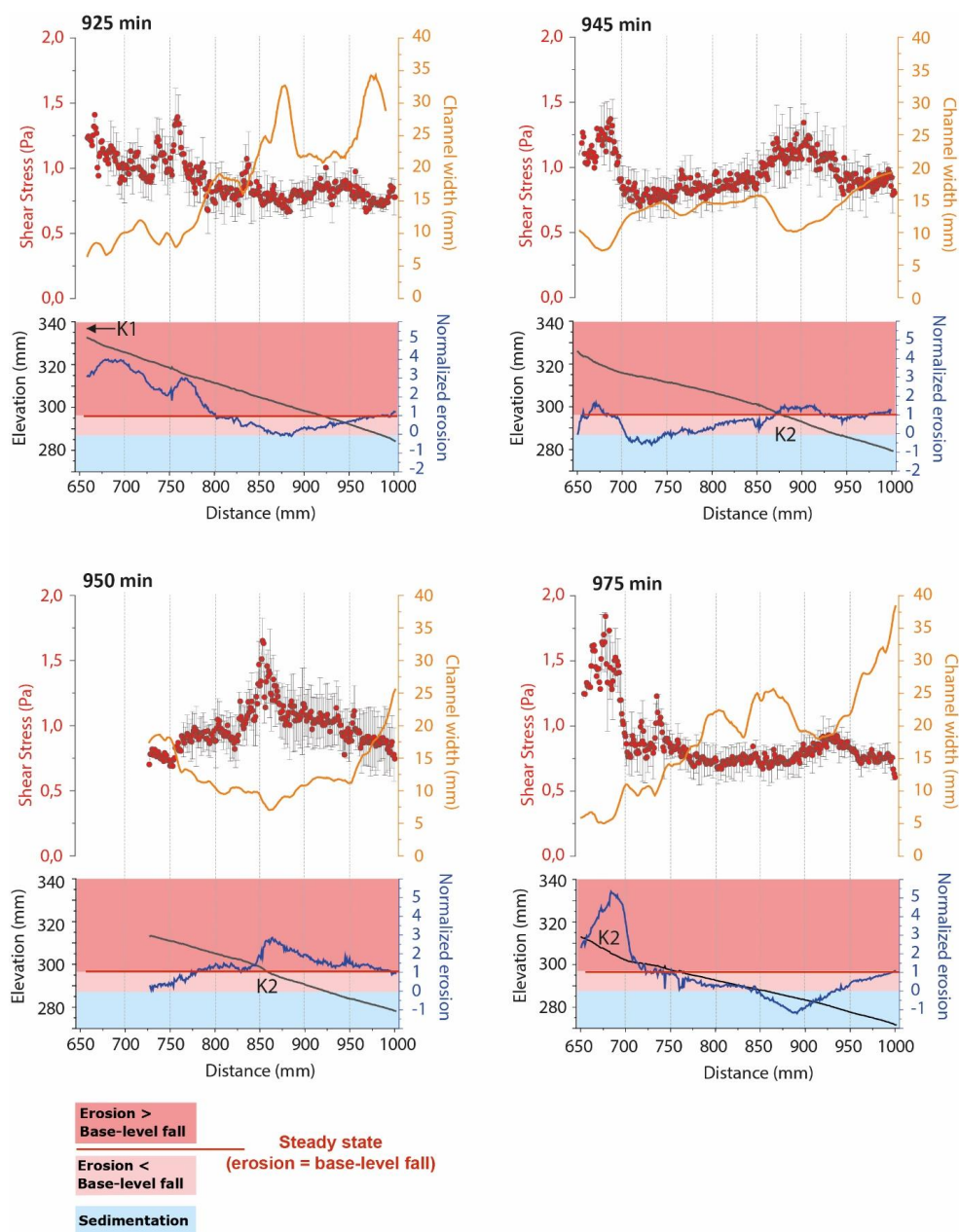


308

309 **Figure 11.** Time-series at 5 min interval of river width (A) and unit and total discharge (B) for the
 310 channel in experiment MBV06 shown in Figure 10B. Time-series of box-and-whisker plots of normalized
 311 elevation changes (C) and shear stress (FD) for all pixels across the section. Orange solid circles and
 312 yellow lines show the mean and median values respectively. Edges of the boxes indicate the 25th and
 313 75th percentiles. Crosshatched areas indicate the passage of knickpoints.



314 To complement cross-section data, we show in Figure 12 how parameters vary longitudinal by
315 considering four stages, two before (925 min) and after (975 min) the passage of the second knickpoint
316 and two during its retreat (945 and 950 min). Note that at 925 min, the first knickpoint (K1) has just
317 passed upstream the investigated profile and is responsible for the enhanced normalized erosion and
318 increased shear stress between distance 800 to 650 mm. Similarly, at 975 min the second knickpoint
319 (K2) is still in the upstream part of the profile, between distance 700 to 650 mm. We also reported the
320 longitudinal variations in river width, shear stress and normalized erosion along the profiles. At runtimes
321 925 and 975 min, after the passage of a knickpoint, erosion is below the BL rate along all the profiles
322 down the knickpoints, with even localized sedimentation at 975 min between 805 and ~950 mm. These
323 sections are characterized by low shear stress values, being between 0.5 and 1 and by rivers that widen
324 downward (around 0.7 mm/cm). On the opposite, during the passage of a second knickpoint (K2) at
325 runtimes 945 and 950 min, mean shear stress increases locally at the knickpoint location, being > 1 and
326 the normalized erosion overpasses the BL rate there. These knickpoint segments are characterized by a
327 narrowing of the rivers as already shown previously. The data illustrate that erosion mainly occurs
328 during periods of knickpoint retreat though a combination of local steepening of the profile and
329 narrowing of the river, resulting in an increase shear stress. On the opposite, once a knickpoint has and
330 between the passage of two successive knickpoints, erosion decreases significantly and does not longer
331 compensate the BL fall. These periods of defeated erosion are characterized by low bed shear stress
332 values in wide rivers, that widen downward.



333

334 **Figure 12.** Longitudinal trends of hydro-geomorphic parameters in experiment MBV 06 at runtimes

335 925, 945, 950 and 975 min (see text for comments). K1 and K2: first and second knickpoints discussed

336 in the text (see also Fig. 10A).



337 **4 Discussion and conclusions**

338 Our experiments illustrate the generation and retreat of successive knickpoint waves that traveled across
339 the landscape during the growth of drainage networks. They formed throughout the duration of
340 experiments regardless of the steadiness of the precipitation and BL fall rates and of the homogeneity
341 of the eroded material. Consequently, these knickpoints were autogenically generated (Hasbargen and
342 Paola, 2000), arising only from internal geomorphic adjustments within the catchments rather than from
343 variation in external forcing. Our observations appear very similar to those of Hasbargen and Paola
344 (2000, 2003) and Bigi et al. (2006) who also reported the generation of successive knickpoints in
345 landscape experiments evolving under steady forcing (rainfall and BL fall rate), throughout the duration
346 of the runs. These authors mentioned that their initiation was not “*attributed to abrupt base-level drops,*
347 *because the outlet drops continuously*” (Hasbargen and Paola, 2000) as in our study. Unlike our
348 experiments, which mainly consider the growth phase of the drainage networks, experiments reported
349 in Hasbargen and Paola (2000, 2003) and Bigi et al. (2006) considered the propagation of knickpoints
350 after the phase of network growth, while their system was at steady-state in average (mean catchment
351 erosion rate equal to BL rate). Then, given that the size of their experimental catchment was steady over
352 time and given the steady rainfall rate, they were able to rule out variations of water discharge over time
353 as the main driver for the generation of their knickpoints. On the opposite, in our experiments the size
354 of catchments continuously increased over time, and thus the water discharge. However, this does not
355 appear as the main factor controlling knickpoints initiation for several reasons. First, as we already
356 mentioned, knickpoints arose at all stages of network growth and divide retreat, for both small and large
357 rivers (Fig. 7), and thus whatever the range of water discharge at outlet. Second, the migration of the
358 water divide related to drainage network growth occurred steadily and roughly at a constant rate during
359 an experiment (see Figures 5 and 7), and then the size of the catchments and the related increase in water
360 discharge. Then, we can rule out abrupt variations in discharge as the driving mechanism for knickpoint
361 initiation. Last, knickpoint initiations occurred at a higher frequency than the increase in water discharge
362 that results from catchment expansion and divide migration. For example, in addition to unit discharge,
363 we also reported on Figure 11C the variation in total discharge during the 120 min-long sequence of

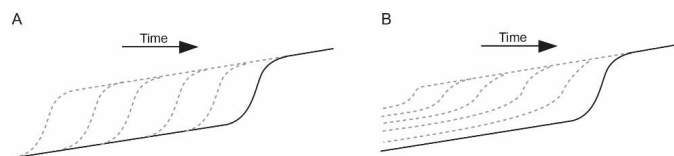


364 knickpoint initiation discussed previously. The total discharge rose from $3.7 \cdot 10^7$ to $4.0 \cdot 10^7$ $\text{mm}^3 \cdot \text{h}^{-1}$ in
365 120 minutes representing a $\sim 8\%$ increase, which is relatively low compared to the $\sim 100\%$ increase of
366 unit discharge during the passage of a knickpoint. For all these reasons we conclude that the change in
367 catchment size was not the main driver of successive knickpoints initiation in our experiments, which
368 occurs at a higher frequency.

369 Admitting that the initiation of successive knickpoints was not related to changes in external factors and
370 catchment size over time, it is then necessary to consider internal geomorphic processes as driving
371 mechanisms. The detailed sequence of knickpoints initiation and propagation discussed above clearly
372 shows enhanced incision above BL fall during the periods of knickpoints propagation. This occurred
373 through local steepening of the longitudinal profile and narrowing of the river, these two factors leading
374 to an increase in unit discharge and bed shear stress along the knickpoint section. Several studies already
375 documented how steepening and narrowing act together for increasing river incision rate (e.g. Lavé and
376 Avouac, 2001; Duvall et al., 2004; Whittaker et al., 2007; Cook et al., 2013), which is what we also
377 document here. The particularity of the rivers in our study however lies in the phase of post-knickpoint
378 retreat. Actually, immediately after the retreat of a knickpoint, erosion was inhibited downstream and
379 rivers no longer incised despite the ongoing BL fall, until the passage of a new knickpoint. Although
380 clearly shown in the sequence detailed previously (Figs. 10 to 12), this was a general behavior that
381 concerned the three experiments presented here and their whole longitudinal profile, not only their
382 downstream part as in the sequence discussed above. Actually, this systematic defeat in erosion
383 downstream the knickpoints is inherent to the geometry of the stacks of all successive longitudinal
384 profiles of each experiment shown in Figure 6. In most cases, profiles downstream retreating knickpoints
385 stack on top of each other, as illustrated schematically on Figure 13A, which indicates minor or no
386 erosion downstream the knickpoints. In the case of continuous adjustment of rivers to BL fall
387 downstream knickpoints, the geometry of profiles should rather shows a pattern as illustrated in Figure
388 13B. The pattern of profiles evolution over time documented here is usually observed following a sudden
389 and finite drop in BL (Finnegan, 2013; Grimaud et al., 2016) and to our best knowledge this is the first
390 time here that such geometry is documented in the case of a continuous BL fall. This particular pattern

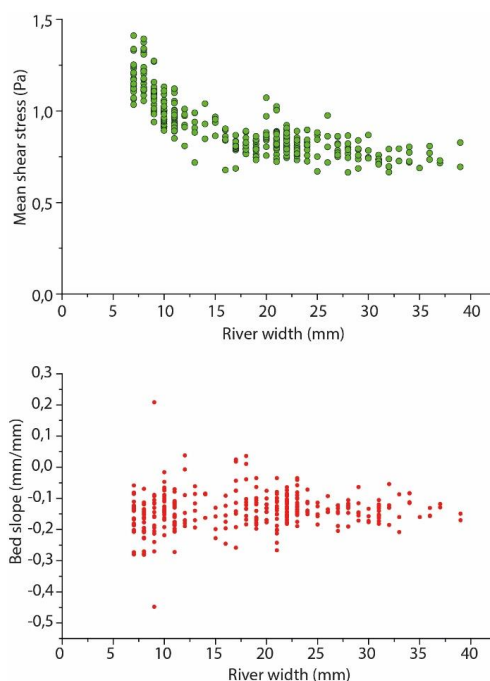


391 is explained by the decrease in erosion rate downstream the retreating knickpoints which finally acts as
392 if the BL was not falling continuously at a constant rate but dropped regularly step-by-step. Therefore,
393 understanding the systematic occurrence of successive knickpoints in our experiments requires to
394 understand why erosion rate dropped downstream of knickpoints following their retreat. After the
395 passage of knickpoints, we systematically observe a widening of the rivers, as also documented in
396 natural systems (e.g. Cook et al., 2014; Zavala-Ortiz et al., 2021) and a decrease in the bed shear stress.
397 Because an increase in channel width over time will inevitably reduce the bed shear stress if discharge
398 and river gradient remain constant (Fuller et al., 2016), we propose that widening was the main factor
399 responsible for the decrease in shear stress and erosion rate after the passage of a knickpoint, and then
400 for the occurrence of the successive autogenic knickpoints. Demonstrating the sole effect of river width
401 on bed shear stress and erosion rate is complicated by covariations of these factors with river slope and
402 variations of discharge related to connection of tributaries. This can be discussed however on the basis
403 of the sequence discussed previously, particularly at runtime 925 min between the passage of two
404 successive knickpoints (Figs. 10 and 12). At that time, the profile of the river had a roughly constant
405 slope, without any slope break (Fig. 14) and no major tributary connected (Fig. 10) that could change
406 significantly the water discharge. As illustrated in Figure 12, this river segment was characterized by
407 widening and decreasing shear stress downward. Then, as shown in Figure 14 we can document here a
408 decrease in shear stress that was only the result of the widening of the river downward. This observation
409 supports our hypothesis that defeated erosion downstream the propagating knickpoints was mainly due
410 to the widening dynamics of the experimental rivers.



411

412 **Figure 13.** Sketches illustrating the difference in the geometry of successive longitudinal profiles
413 following the retreat of a knickpoint depending on whether fluvial incision is inhibited (A) or not (B)
414 downstream of the retreating knickpoint.



415

416 **Figure 14.** Top: river bed shear stress according to river width in the downstream section, 40 cm-long,
417 of experiment MBV06 at runtime 925 (see also Fig.12). Bottom: corresponding slope of the river bed.

418

419 The set of experiments presented here illustrates the initiation and propagation of successive knickpoints
420 during the growth of drainage networks and progressing enlargement of catchments, under constant
421 external forcing. From the detailed analysis of their initiation and propagation, we propose that they
422 formed autogenically, in response to variations in river width. We show that once knickpoints had
423 retreated, unit discharge, shear stress and incision rate all decreased downstream while the rivers
424 widened, resulting in a state where incision no longer counterbalanced the BL fall. We propose that
425 rivers widening downstream the retreating knickpoints is the main mechanism responsible for the
426 decrease in incision rate through its feedback on unit discharge and shear stress. This results in an
427 unstable situation that ends up with the initiation and propagation of a new knickpoint and a sequence
428 of river narrowing, increasing shear stress and incision rate. Then, incision of rivers in these experiments
429 appears to be fundamentally discontinuous despite continuous forcing, and we highlight downstream



430 river width dynamics as the main driver. Unlike studies that documented how river narrowing leads to
431 an increase in shear stress and incision rate (Lavé and Avouac, 2001; Duvall et al., 2004; Whittaker et
432 al., 2007; Cook et al., 2013) we propose that the opposite, river widening, is potentially responsible for
433 a decrease in erosion rate downstream a retreating knickpoint, leading ultimately to the generation of a
434 new knickpoint. This specific mode of autogenic knickpoints initiation result in an upward dynamic of
435 retreat that is not conventional, as we observe that they first accelerate during the first step of their
436 propagation before to decelerate in a second time as they approach the divide. Actually, studies that
437 investigated knickpoints retreat at catchment-scale due to a single drop of base-level (due to a fault that
438 displaced the river bed or to a capture for example) show that their velocity decreases as they propagate
439 upstream due to the progressive reduction of the upstream drainage area and water discharge (e.g.
440 Crosby and Whipple, 2006. Berlin and Anderson, 2007). The specific mode of retreat dynamics that we
441 document here is likely the consequence of their specific mode of initiation. Although further studies
442 should be conducted on this question, we found that the maximum retreat velocity (which scales with
443 the rate of BL fall) occurs in the mid of the catchments in all our experiments, whatever the rate of BF
444 fall and the length of the rivers. This appears as a key element for understanding the dynamics of these
445 knickpoints.

446 Knickpoints are commonly linked to variations in tectonics or climate through their influence on base
447 level and/or sediment supply (e.g. Whipple and Tucker, 1999; Crosby and Whipple, 2006; Kirby and
448 Whipple, 2012; Whittaker and Boulton, 2012). The recognition that knickpoints may be generated
449 autogenically in relationship to river width dynamics is then of first importance for investigating how
450 tectonics and climate impact landscape and erosion. The generation of autogenic knickpoints has already
451 been observed in experiments that evolved under steady forcing (Hasbargen and Paola, 2000, 2003; Bigi
452 et al., 2006) and ascribed to water flow close to critical conditions by Hasbargen and Paola (2000). Our
453 model is consistent with this proposition. By performing such exploratory experiments, we do not
454 pretend to reproduce natural landscapes in the laboratory because of important scaling issues (see Paola
455 et al., 2009 for an extensive reflection on this matter) but rather to highlight and document complex
456 system behaviors under controlled conditions that could provoke further investigations. For instance,



457 the dynamics observed here could not be reproduced in numerical simulations based on a classical
458 Stream Power Incision model that would not integrate a dynamic width (see Lague, 2014), which
459 appears as key ingredient here and supports ongoing investigations on this topic (e.g. Turowski, 2018;
460 Croissant et al., 2019; Baynes et al., 2020).

461

462 **Author contributions.** SB designed the experimental device. LdL, SB and AG built the experimental
463 setup and carried out the experiments. LdL analyzed the data with the help of SB and PhD. All authors
464 discussed the data. LdL and SB wrote the manuscript with input from AG and PhD.

465

466 **Acknowledgements.** This work was supported by ORANO-Malvesi. We thank Sebastien Carretier
467 and Odin Marc for fruitful discussions and Jens Turowski for his comments on a preliminary version
468 of this manuscript.

469

470 **References**

471 Baynes, E.R.C., Lague, D., Attal, M., Gangloff, A., Kirstein, L.A., and Dugmore, A.J.: River self-
472 organisation inhibits discharge control on waterfall migration: Scientific Reports, v. 8, p. 2444,
473 doi:10.1038/s41598-018-20767-6, 2018.

474 Baynes, E.R.C., Lague, D., Steer, P., Bonnet, S., and Illien, L.: Sediment flux-driven channel
475 geometry adjustment of bedrock and mixed gravel–bedrock rivers: Earth Surface Processes and
476 Landforms, v. 45, p. 3714–3731, doi:10.1002/esp.4996, 2020.

477 Berlin, M.M., and Anderson, R.S.: Modeling of knickpoint retreat on the Roan Plateau, western
478 Colorado: Journal of Geophysical Research, v. 112, p. F03S06, doi:10.1029/2006JF000553, 2007.

479 Bigi, A., Hasbargen, L.E., Montarani, A., and Paola, C.: Knickpoints and hillslope failure: Interactions
480 in a steady-state experimental landscape, *in* Willet, C.D., Hovius, N., Brandon, M.T., and Fisher,



- 481 D.M., eds. Tectonics, Climate and Landscape evolution: Geological Society of America Special paper
482 398, p. 295-307, doi:10.1130/2006.2398(18), 2006.
- 483 Bonnet, S.: Shrinking and splitting of drainage basins in orogenic landscapes from the migration of the
484 main drainage divide: *Nature Geoscience*, v. 2, p. 766–771, doi:10.1038/ngeo666, 2009.
- 485 Bonnet, S., and Crave, A.: Landscape response to climate change: Insights from experimental
486 modeling and implications for tectonic versus climatic uplift of topography: *Geology*, v. 31, p. 123–
487 126, doi: 10.1130/0091–7613, 2003.
- 488 Cantelli, A., and Muto, T.: Multiple knickpoints in an alluvial river generated by a single drop in base
489 level: experimental investigation: *Earth Surface Dynamics*, 2, 271-278, doi:10.5194/esurf-2-271-2014,
490 2014.
- 491 Cook, K.L., Turowski, J.M., and Hovius, N.: A demonstration of the importance of bedload transport
492 for fluvial bedrock erosion and knickpoint propagation: *Earth Surface Processes and Landforms*, v. 38,
493 p. 683–695, doi:10.1002/esp.3313, 2013.
- 494 Cook, K.L., Turowski, J.M., and Hovius, N.: River gorge eradication by downstream sweep erosion:
495 *Nature geoscience*, doi:10.1038/NGEO2224, 2014.
- 496 Croissant, T., Lague, D., and Davy, P.: Channel widening downstream of valley gorges influenced by
497 flood frequency and floodplain roughness: *Journal of Geophysical Research-Earth Surface*, v. 124, p.
498 154–174, doi:10.1029/2018JF004767, 2019.
- 499 Crosby, B.T., and Whipple, K.X.: Knickpoint initiation and distribution within fluvial networks: 236
500 waterfalls in the Waipaoa River, North Island, New Zealand: *Geomorphology*, v. 82, p. 16–38,
501 doi:10.1016/j.geomorph.2005.08.023, 2006.
- 502 Davy, P., Croissant, T., and Lague, D.: A precipitation method to calculate river hydrodynamics, with
503 applications to flood prediction, landscape evolution models, and braiding instabilities: *Journal of*
504 *Geophysical Research-Earth Surface*, v. 122, p. 1491–1512, doi:10.1002/2016JF004156, 2017.



- 505 Duvall, A., Kirby, E., and Burbank, D.: Tectonic and lithologic controls on bedrock channel profiles
506 and processes in coastal California: *Journal of Geophysical Research*, v. 109, p. F03002,
507 doi:10.1029/2003JF000086, 2004.
- 508 Finnegan, N.J.: Interpretation and downstream correlation of bedrock river terrace treads created by
509 propagation knickpoints: *Journal of Geophysical Research-Earth Surface*, v. 118,
510 doi:10.1029/2012JF002534, 2013.
- 511 Finnegan, N.J., and Dietrich, W.E.: Episodic bedrock strath terrace formation due to meander
512 migration and cutoff: *Geology*, 39, 143-146, doi:10.1130/G31716.1, 2011.
- 513 Fuller, T.K., Gran, K.B., Sklar, L.S., and Paola, C.: Lateral erosion in an experimental bedrock
514 channel: The influence of bed roughness on erosion by bed load impacts: *Journal of Geophysical*
515 *Research-Earth Surface*, v. 121, p. 1084-1105, doi:10.1002/2015JF003728, 2016.
- 516 Grimaud, J.-L., Paola, C., and Voller, V.: Experimental migration of knickpoints: influence of style of
517 base-level fall and bed lithology: *Earth Surface Dynamics*, v. 4, p. 11–23, doi:10.5194/esurf-4-11-
518 2016, 2016.
- 519 Hancock, G.S., and Anderson, R.S.: Numerical modeling of fluvial strath-terrace formation in
520 response to oscillating climate: *Geological Society of America Bulletin*, v. 114, p. 1131-1142, 2000.
- 521 Hasbargen, L.E., and Paola, C.: Landscape instability in an experimental drainage basin: *Geology*, v.
522 24, p. 1067-1070, 2000.
- 523 Hasbargen, L.E., and Paola, C.: How predictable is local erosion rate in erosional landscape ? *in*
524 Wilcox, P.R. and Iverson, R.M., eds., *Prediction in Geomorphology: American Geophysical Union*
525 *Geophysical Monograph* 135, doi:10.1029/135GM16, 2003.
- 526 Hilley, G.E., and Arrowsmith, J.R.: Geomorphic response to uplift along the Dragon's Back pressure
527 ridge, Carrizo Plain, California: *Geology*, v. 36, p. 367-370, doi:10.1130/G24517A.1, 2008.
- 528 Kirby, E., and Whipple, K.X.: Expression of active tectonics in erosional landscapes: *Journal of*
529 *Structural Geology*, v. 44, p. 54–75, doi:10.1016/j.jsg.2012.07.009, 2012.



- 530 Lague, D.: The stream power river incision model: evidence, theory and beyond: *Earth Surface*
531 *Processes and Landforms*, v. 39, p. 38–61, doi:10.1002/esp.3462, 2014.
- 532 Lague, D., Crave, A., and Davy, P.: Laboratory experiments simulating the geomorphic response to
533 tectonic uplift: *Journal of Geophysical Research-Solid Earth*, v. 108, doi:10.1029/2002JB001785,
534 2003.
- 535 Lavé, J., and Avouac, J.P.: Fluvial incision and tectonic uplift across the Himalayas of central Nepal:
536 *Journal of Geophysical Research-Solid Earth*, v. 106, p. 26561–26591, doi:10.1029/2001JB000359,
537 2001.
- 538 Mitchell, N.A., and Yanites, B.J.: Spatially variable increase in rock uplift in the Northern U.S.
539 Cordillera recorded in the distribution of river knickpoint and incision depths: *Journal of Geophysical*
540 *Research: Earth Surface*, v. 124, 1238–1260, doi:10.1029/2018JF004880, 2019.
- 541 Moussirou, B., and Bonnet, S.: Modulation of the erosion rate of an uplifting landscape by long-term
542 climate change: An experimental investigation: *Geomorphology*, v. 303, p. 456–466,
543 doi:10.1016/j.geomorph.2017.12.010, 2018.
- 544 Paola, C., Straub, K., Mohrig, D., and Reinhardt, L.: The “unreasonable effectiveness” of stratigraphic
545 and geomorphic experiments: *Earth-Science Reviews*, v. 97, p. 1–43,
546 doi:10.1016/j.earscirev.2009.05.003, 2009.
- 547 Rohais, S., Bonnet, S., and Eschard, R.: Sedimentary record of tectonic and climatic erosional
548 perturbations in an experimental coupled catchment-fan system: *Basin Research*, v. 24, p. 198–212,
549 doi:10.1111/j.1365-2117.2011.00520.x, 2012.
- 550 Scheingross, J.S., Lamb, M.P., and Fuller, B.M.: Self-formed bedrock waterfalls: *Nature*, v. 567, p.
551 229–233, doi:10.1038/s41586-019-0991-z, 2019.
- 552 Singh, A., Reinhardt, L., and Foufoula-Georgiou, E.: Landscape reorganization under changing
553 climatic forcing: Results from an experimental landscape: *Water Resources Research*, v. 51, p. 4320–
554 4337, doi:10.1002/2015WR017161, 2015.



- 555 Sweeney, K.E., Roering, J.J., and Ellis, C.: Experimental evidence for hillslope control of landscape
556 scale: *Science*, v. 349, p. 51–53, doi:10.1126/science.aab0017, 2015.
- 557 Tofelde, S., Savi, S., Wickert, A. D., Bufe, A., and Schildgen, T. F.: Alluvial channel response to
558 environmental perturbations: fill-terrace formation and sediment-signal disruption. *Earth Surface*
559 *Dynamics*, v. 7, p. 609-631, doi:10.5194/esurf-7-609-2019, 2019.
- 560 Turowski, J.M.: Alluvial cover controlling the width, slope and sinuosity of bedrock channels: *Earth*
561 *Surface Dynamics*, v. 6, p. 29–48, doi:10.5194/esurf-6-29-2018, 2018.
- 562 Turowski, J.M., Lague, D., Crave, A., and Hovius, N.: Experimental channel response to tectonic
563 uplift: *Journal of Geophysical Research-Earth Surface*, v. 111, doi:10.1029/2005JF000306, 2006.
- 564 Whipple, K.X., and Tucker, G.E.: Dynamics of the stream-power river incision model: Im-
565 plications for height limits of mountain ranges, landscape response timescales, and research needs: *Journal of*
566 *Geophysical Research*, v. 104, p. 17,661–17,674, 1999.
- 567 Whittaker, A.C., and Boulton, S.J.: Tectonic and climatic controls on knickpoint retreat rates and
568 landscape response times: *Journal of Geophysical Research*, v. 117, F02024, doi:10
569 .1029/2011JF002157, 2012.
- 570 Whittaker, A.C., Cowie, P.A., Attal, M., Tucker, G.E., and Roberts, G.P.: Bedrock channel adjustment
571 to tectonic forcing: Implications for predicting river incision rates: *Geology*, v. 35, p. 103,
572 doi:10.1130/G23106A.1, 2007.
- 573 Yanites, B.J., Ehlers, T.A., Becker, J.K., Schnellmann, M., and Heuberger, S.: High magnitude and
574 rapid incision from river capture: Rhine River, Switzerland: *Journal of Geophysical Research*, v. 118,
575 1-25, doi:10.1002/jgrf200567, 2013.
- 576 Zavala-Ortiz, V., Carretier, S., Regard, V., Bonnet, S., Riquelme, R., and Choy, S.: Along-stream
577 variations in valley flank erosion rates measured using ^{10}Be concentrations in colluvial deposits from
578 canyons in the Atacama Desert: *Geophysical Research Letters*, 48, doi:10.1029/2020GL089961, 2021.